Electrochimica Acta, Vol. 38, No. 11, pp. 1513–1520, 1993
Printed in Great Britain.

0013–4686/93 $6.00 + 0.00

KINETICS AND MECHANISM OF $PbSO_4$ ELECTROFORMATION ON Pb ELECTRODES IN H_2SO_4 AQUEOUS SOLUTIONS

F. E. VARELA, M. E. VELA, J. R. VILCHE and A. J. ARVIA

Instituto de Investigaciones Fisicoquímicas Teóricas y Aplicadas (INIFTA), Facultad de Ciencias Exactas, Universidad Nacional de La Plata, Sucursal 4, Casilla de Correo 16, (1900) La Plata, Argentina

(*Received* 17 *November* 1992; *in revised form* 25 *January* 1993)

Abstract—The electrochemical processes related to the passivation of Pb in 5 M H_2SO_4 at 25°C, have been investigated combining a rotating ring-disk electrode, linear potential sweep voltammetry and potentiostatic pulse techniques complemented with scanning electron microscopic imaging. The kinetics of $PbSO_4$ anodic layer growth can be explained through the initial formation of a barrier layer acting as an ionic conductor, and the transference of Pb^{2+} cations from the substrate through the conducting layer yielding Pb^{2+} ion in the solution. These ions further contribute to passivation through the precipitation of a $PbSO_4$ passivating layer.

Key words: lead/sulphuric acid system, lead electro-oxidation, nucleation and growth of lead sulphate, lead passivation, lead soluble species.

INTRODUCTION

The kinetics and mechanism of $PbSO_4$ formation on Pb electrodes in concentrated suphuric acid solutions were rather extensively studied over the past three decades[1–14]. However, the electrochemical processes leading to the formation of $PbSO_4$ on Pb have been ambiguously explained. There are still some discrepancies between the influence of certain variables on the global process[5, 7, 9], such as the electrode surface preparation[5, 13, 14] and the hydrodynamic conditions[5, 14].

In general, the interpretation of kinetic data has been based upon three main reaction models[7, 14]. (i) A dissolution–precipitation mechanism[5] in which the $PbSO_4$ nuclei are formed in the solution adjacent to Pb surface, the growth of the three-dimensional $PbSO_4$ layer occurs through the Pb electrodissolution and subsequent incorporation of soluble Pb^{2+} species into growing nuclei. In this case Pb passivation is attributed to a surface blockage by $PbSO_4$. (ii) A solid-state mechanism[11], involving $PbSO_4$ nucleation and either a two- or three-dimensional $PbSO_4$ layer growth on a Pb surface[6, 11], until this surface becomes mostly covered by the $PbSO_4$ layer. The subsequent growth of the $PbSO_4$ layer involves the transport of Pb^{2+} ions through the $PbSO_4$ layer. It appears that mechanism (i) is valid for Pb passivation at relatively low anodic overpotentials, whereas mechanism (ii) predominates at high anodic overpotentials. (iii) A complex mechanism for explaining the $PbSO_4$ formation during Pb anodization in aqueous sulphuric acid includes the nucleation and growth of $PbSO_4$ occurring in parallel with Pb electrodissolution yielding soluble Pb^{2+} species[15, 16]. This mechanism implies the formation of a thin ionically conducting barrier, which assists the migration of Pb^{2+} ions. This explanation was firstly advanced by Pavlov[8] and Pavlov and Popova[9] who admitted that at positive potentials the inner part of the $PbSO_4$ layer acted simultaneously as a perm-selective membrane for Pb^{2+} ions, and as a blocking membrane for the access of SO_4^{2-} ions to the interfacial region. A further growth of the $PbSO_4$ layer requires the diffusion of Pb^{2+} ions through the $PbSO_4$ layer and their subsequent precipitation as $PbSO_4$.

This paper examines Pb electrodissolution and passivation in H_2SO_4 aqueous solutions combining a rotating ring-disc electrode, linear potential sweep voltammetry and potentiostatic current transient techniques complemented with scanning electron microscopy (SEM). The parametric analysis using non-linear least-square fit routines allows us to advance an interpretation of the electroformation of $PbSO_4$ layers which can be considered as an improvement of mechanism (iii)[15, 16].

EXPERIMENTAL

The experimental setup has been described in previous publications[17–19]. Working electrodes were made of "Specpure" lead (Johnson Matthey) in the form of a rotating disc electrode mounted as a Pb ring–Pb disc rotating electrode device (*rrde*). The Pb disc diameter was $r_d = 4.5$ mm, and the inner and outer Pb ring diameters were $r_{ir} = 4.9$ mm and $r_{or} = 5.3$ mm, respectively. The collection efficiency of this setup was $N_T = 0.202$[20]. Before each electrochemical run, the *rrde* was mechanically polished with 600 and 1200 grade emery papers, and afterwards thoroughly rinsed with triply-distilled water. Finally, the Pb disc electrode was polarized for 5 min by setting the potential in the hydrogen evolution potential range, in order to provide a reproducible electroreduced Pb initial surface. For the sake of comparison, after the mechanical polishing, a number of

specimens were subjected to either a chemical etching in 20% H_2O_2 (100 vol.) + 80% glacial acetic acid solution followed by rinsing in methanol, or a 10 s electropolishing in 40% $NaBF_4$ + 2% H_2SO_4 at 0.6 A dm^{-2}.

The electrochemical cell was completed with a large area Pt counter electrode and a $Hg/Hg_2SO_4/K_2SO_4$ (saturated) reference electrode (E_r/V (vs. *nhe*) = 0.680) properly shielded and connected to the rest of the cell through a Luggin–Haber capillary tip. Potentials in the text are given against the $Hg/Hg_2SO_4/K_2SO_4$ (saturated) electrode (Hg*se*).

The following aqueous electrolyte solutions were used, 5 M H_2SO_4, 0.5 M H_2SO_4 (pH 0.3) and 0.5 M $(NH_4)_2SO_4$ + 5 × 10^{-4} M H_2SO_4 (pH 3). These solutions were prepared from analytical grade (p.a. Merck) reagents and Milli-Q* water. Runs were performed under N_2 gas saturation at 25°C.

Experiments were made following two main procedures. In the first one, the *rrde* electrode was subjected to either a single (STPS) or a repetitive (RTPS) triangular potential sweep between the cathodic ($E_{s,c}$) and the anodic ($E_{s,a}$) switching potentials at a scan rate (v) comprised in the $7 \times 10^{-5} \leqslant v \leqslant 0.2\,V\,s^{-1}$ range, under either a stationary or a rotation condition (ω) up to $\omega = 2600$ rpm. In the second procedure a potential step from $E_{s,c}$ to E_f ($-1.015 \leqslant E_f \leqslant -0.880$ V) was applied and the corresponding anodic current transient at $\omega = 1000$ rpm was recorded, the ring electrode being held at $E_R = -1.100$ V to detect soluble Pb species produced at the disc. The different potential routines are illustrated as insets in the figures. After the electrochemical measurements the electrodes were washed with triply distilled water and stored in a vacuum desiccator. For SEM observations the samples were coated with a thin layer of gold by diode sputtering and they were examined using a Philips 500 scanning electron microscope.

RESULTS

1. *Voltammetric data*

Voltammograms of Pb in 5 M H_2SO_4 run between $E_{s,c} = -1.350$ V and $E_{s,a} = -0.800$ V within the $0.002 \leqslant v \leqslant 0.200\,V\,s^{-1}$ range, as jv^{-1} vs. E plots, are shown in Fig. 1. The positive going potential scan exhibits a well defined anodic current peak (A1) corresponding to the electro-oxidation of Pb–Pb(II) followed by a wide passive current region[19]. The reverse scan shows an asymmetric cathodic peak (C1) which is related to the electroreduction of Pb(II)-containing species. The initiation of both peaks A1 and C1 is close to the reversible potential of the $Pb/PbSO_4$ electrode $E_{Pb/PbSO_4/5\,M\,H_2SO_4}$/V (vs. Hg*se*) = −1.036, at 25°C[21].

The jv^{-1} vs. E plots show that as v is decreased, $j_{p,A1}$ and $j_{p,C1}$, the heights of peaks A1 and C1 increase, *ie* the voltammetric charge, either anodic or cathodic increases (Fig. 2). The dependences of the overall anodic (q_a) and cathodic (q_c) apparent charge densities are plotted against v in Fig. 2a–b. At first, the q_a vs. $v^{-1/2}$ linear dependence may suggest that the anodic reaction behaves as a diffusion controlled electrochemical process, but the non-zero value of q_a for $v \Rightarrow \infty$ (Fig. 2a) points out that the process also

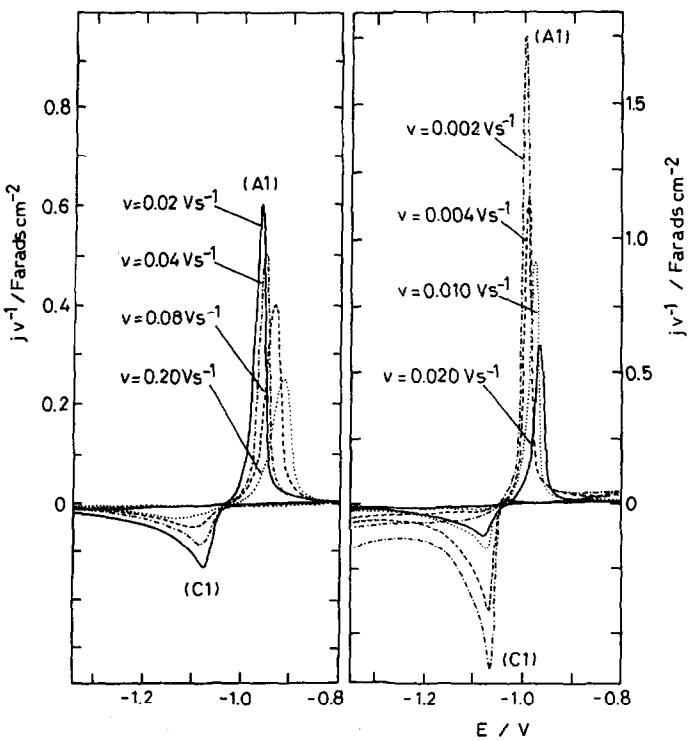

Fig. 1. Voltammetric data depicted as jv^{-1} vs. E plots at different v in 5 M H_2SO_4, 25°C. $E_{s,c}$ = −1.35 V, $E_{s,a}$ = −0.80 V. Unstirred solution.

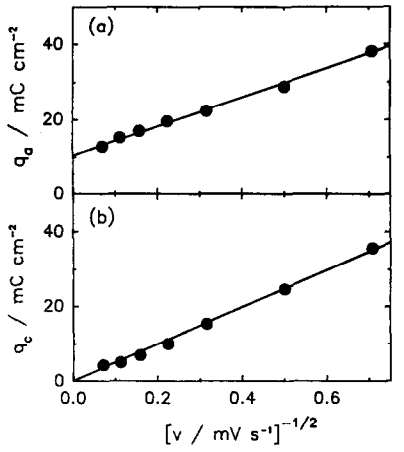

Fig. 2. Dependence of (a) q_a and (b) q_c on $v^{-1/2}$. Data obtained from voltammograms run between $E_{s,c} = -1.35$ V and $E_{s,a} = -0.80$ V in the $0.002 \leqslant v \leqslant 0.200$ V s^{-1} range, in 5 M H_2SO_4, 25°C. Unstirred solution.

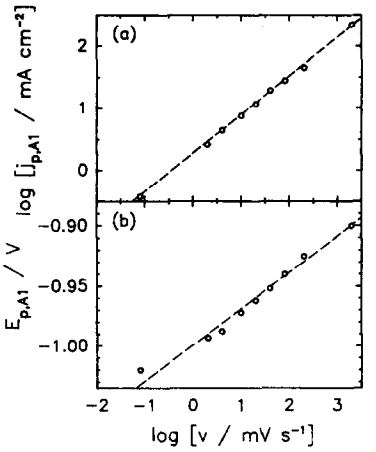

Fig. 3. Dependences of (a) $j_{p,A1}$ and (b) $E_{p,A1}$ on log v. Data obtained from voltammograms run between $E_{s,c} = -1.35$ V and $E_{s,a} = -0.80$ V in the $0.002 \leqslant v \leqslant 0.200$ V s^{-1} range, in 5 M H_2SO_4, 25°C. Unstirred solution.

involves a non-diffusional kinetic contribution. In addition, the log $j_{p,A1}$ vs. log v plot approaches a linear relationship with a slope 0.58 ± 0.04 (Fig. 3a), and the difference between $E_{p,A1}$ and $E_{p,C1}$, the potentials of peaks A1 and C1, diminishes as v is decreased. The $E_{p,A1}$ vs. log v plot exhibits a reasonable linear relationship with the slope 0.032 ± 0.005 V decade^{-1} (Fig. 3b). Furthermore, the potentiodynamic response in the active–passive transition region behaves practically independent of ω; the resistance R defined as the ratio $(\partial E_{p,A1}/\partial v^{1/2})/(\partial j_{p,A1}/\partial v^{1/2})$ results $R = 2.1 \pm 0.3$ Ω cm^2. Accordingly, the voltammetric characteristics of peak A1 exceed the frame of a simple reaction model involving exclusively either diffusion or ohmic resistance kinetic control[22], in contrast to the voltammetric electroreduction of the $PbSO_4$ layer (peak C1) which corresponds to a diffusion controlled process[19].

A voltammogram run at a very low v, *ie* at $v = 7 \times 10^{-5}$ V s^{-1}, from -1.30 V upwards, after holding the working electrode during $\tau_0 = 5$ min at -1.30 V (Fig. 4), shows that the current switches from cathodic to anodic at $E_x = -1.036$ V, a value coinciding with the reversible potential of the $Pb/PbSO_4/H_2SO_4$ electrode[21]. For $E > E_x$ a relatively narrow anodic current plateau followed by a sharp anodic current peak at *ca.* 1.00 V is observed. This peak apparently overlaps the anodic current plateau extending from E_x to *ca.* -0.80 V. Otherwise, when $E > -0.80$ V, the anodic current goes to a smooth minimum at *ca.* -0.40 V, and later it increases slightly up to 0.60 V. These results indicate that there is a certain "induction time", related to the nucleation and growth process of the $PbSO_4$ phase.

The complex voltammetric behaviour of the anodic process suggests the convenience of attempting to separate the direct $PbSO_4$ formation from the

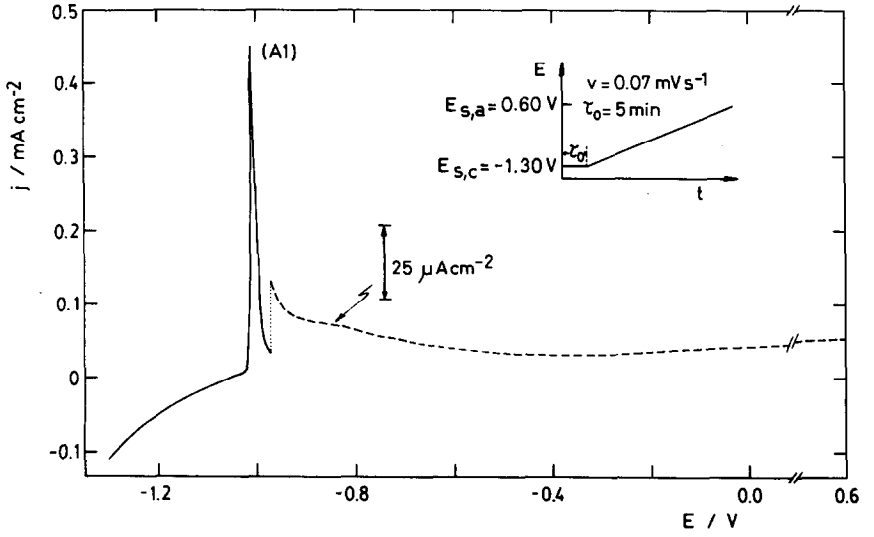

Fig. 4. Voltammogram run at $v = 0.07$ mV s^{-1} between $E_{s,c} = -1.30$ V and $E_{s,c} = 0.60$ V, in 5 M H_2SO_4, 25°C. Unstirred solution.

electro-oxidation of Pb to soluble Pb(II) species, which contributes to a $PbSO_4$ layer further growth.

2. *The formation of* Pb(II) *soluble species during anodization*

The appearance of Pb(II) soluble species during Pb anodization in aqueous sulphuric acid could be observed through voltammetric runs performed with the *rrde* by keeping the Pb ring at $E_R = -1.100$ V (Fig. 5). Thus, Pb(II) soluble species produced at the Pb disc at $v = 0.020\,V\,s^{-1}$, at different values of ω, could be determined through the corresponding electroreduction reaction at the Pb ring electrode.

The voltammograms run with the *rrde* showed that both the height and charge of peak A1 become practically independent of ω, although they decrease in going from the first to the second potential cycle, and simultaneously, the value of $E_{p,A1}$ shifts negatively (Fig. 5a). At $\omega = 1000$ rpm the cathodic current at the ring follows the anodic current at the disc (Fig. 5b). According to these results, there is a clear cathodic current associated with the electroreduction of reaction products originated at the disc. In this case, the current baseline at the ring electrode is related to the steady current of the hydrogen evolution reaction (HER) at E_R. The amount of soluble Pb(II) species produced at the disc lowers considerably along the potential cycling. This behaviour suggests that Pb electrodissolution becomes progressively hindered as the $PbSO_4$ layer is formed during anodization, and that the $PbSO_4$ layer cannot be completely electroreduced to Pb during the cathodic potential scan. It is worth noting that the cathodic current contribution to the ring electrode shows a relatively sharp and somewhat asymmetric peak at $E_D = -0.985$ V, close to the inflection point which can be observed in the ascending branch

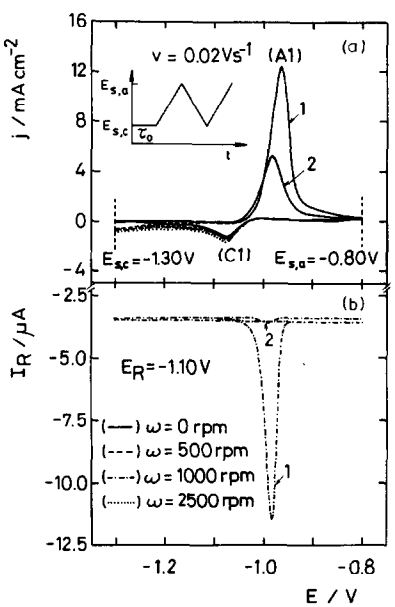

Fig. 5. Voltammetric profiles resulting at the (a) Pb-disc, (b) Pb-ring electrode run between $E_{s,c} = -1.30$ V and $E_{s,a} = -0.80$ V, $v = 0.020\,V\,s^{-1}$, in 5 M H_2SO_4. Rotation speed in the $0 \leqslant \omega \leqslant 2500$ rpm range, $E_R = -1.100$ V, 25°C.

of peak A1 (Fig. 5). From these results and considering the N_T value of the experimental setup, the fraction of the total current related to the generation of Pb(II) soluble species at the disc electrode is about 0.2%. Accordingly, a simple dissolution–precipitation mechanism cannot satisfactorily explain the kinetics of a $PbSO_4$ layer formation on the Pb disc. It appears that a mechanism involving the simultaneous contribution of a nucleation and growth process to the $PbSO_4$ phase formation and the precipitation of Pb(II) soluble species could provide a better explanation of the experimental facts. Further experiments were performed to verify this possibility.

The voltammetric anodic (q_a) and cathodic (q_c) apparent charge densities obtained from the first triangular potential scan depend on the surface pretreatment of Pb electrodes, but this influence practically disappears in the subsequent scans. Thus, for chemically etched Pb electrodes the value of q_a is about 60% the value of q_a resulting from mechanically polished Pb electrodes. Besides, in the former case the $E_{p,A1}$ vs. $v^{1/2}$ and $j_{p,A1}$ vs. $v^{1/2}$ linear plots exhibit the lowest slopes. On the other hand, within the H_2SO_4 concentration and pH ranges covered in this work the kinetics of a $PbSO_4$ layer formation apparently remains independent of the solution composition, except that the $\partial j_p/\partial v^{1/2}$ slope increases as the pH of the electrolyte solution is decreased[22].

3. *Electro-oxidation current transients*

The electro-oxidation current transients were recorded by setting the potential (E_f) in the potential range of peak A1, *ie* $-1.015 \leqslant E_f \leqslant -0.880$ V (Fig. 6, left), the electro-oxidation process at E_f being preceded by a potential step from $E_i = -1.300$ V to E_f. In these transients, the initial current jump due to double layer charging is not observed in the time scale of the figure. This contribution can be neglected as compared to the faradaic charge resulting from current transient integration. Thus, after a minimum current in the ms time scale range has been reached, a peaked value (j_M) at time t_M can be observed. As E_f is shifted positively to value of j_M increases, whereas t_M and q_{Da}, the apparent charge density, decrease (Figs 7 and 8). The current transients become independent of the preceding electroreduction routine when $E_{s,c}$ is set in the -1.40 to -1.20 V range. In general, these current transients resemble those found in either the formation or the disappearance of solid phases at electrochemical interfaces[23].

The current transients at the Pb-ring electrode held at $E_R = -1.100$ V and the anodic current transient at the disc held at E_D were simultaneously recorded. The current transients at the ring (Fig. 6, right) correspond to the electroreduction of Pb(II) species formed at the disc electrode, after correction for the HER current contribution. The current initially increases linearly with time, then reaches a maximum value (j_{RM}) at time t_{RM}, and finally falls to zero. As the value of E_D is shifted up to $E_f = -0.940$ V, the current transient at the ring becomes sharper, and the electroreduction charge derived from these transients diminishes (Fig 6a, b, right).

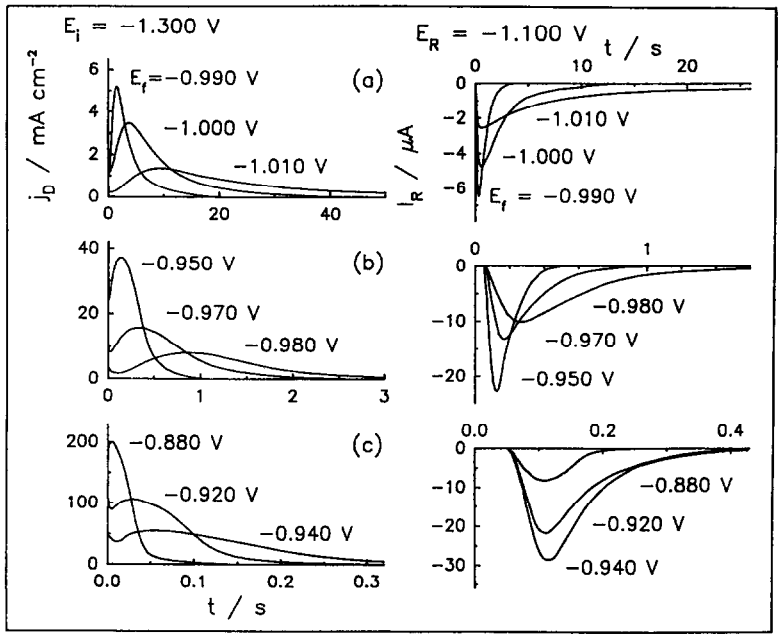

Fig. 6. Disc electrode current transients (left) and the corresponding current transients at the ring electrode (right) recorded at different E_f after a potential holding at $E_i = -1.30$ V during $\tau = 5$ min, in 5 M H_2SO_4, 25°C. $\omega = 1000$ rpm.

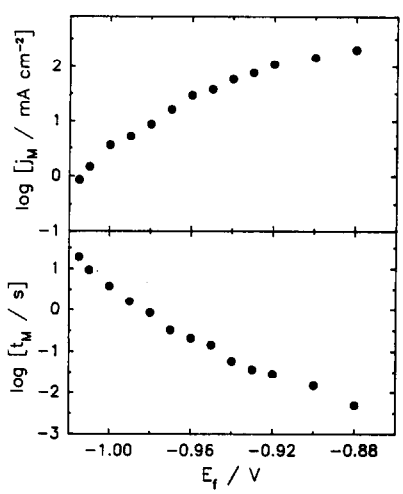

Fig. 7. Dependences of (a) j_M and (b) t_M on E_f. Data derived from current transients recorded under the conditions indicated in Fig. 6.

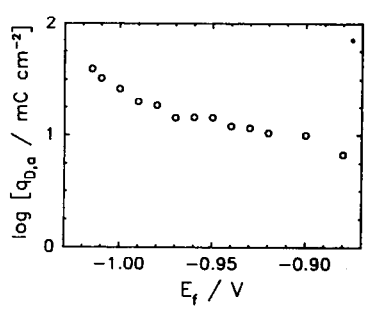

Fig. 8. Dependence of $q_{D,a}$ on E_f. Data derived from current transients at the disc recorded under the conditions indicated in Fig. 6.

But when $E_f > -0.940$ V, the value of j_{RM} decreases although the value of t_{RM} remains independent of E_D (Fig. 6c, right). The lag time (t_R) resulting from the current transients at the disc and at the ring is always close to 50 ms (Fig. 6b, c). This figure can be assigned, in principle, to an ion transport delay and it can be calculated from the equation for a process at the *rrde* under non-stationary conditions[24]:

$$\omega t_R = 43.1(\nu/D)^{1/3}[\log(r_{ir}/r_d)]^{2/3} \quad (1)$$

where ν is the kinematic viscosity of the solution, D is the diffusion coefficient of the reacting species and r_d and r_{ir} are the disc and the ring inner diameter, respectively. Thus, taking 5 M H_2SO_4 at 25°C, $\nu = 0.02$ St, the values r_d and r_{ir} of the *rrde* and ω and t_R from the experiments, it results that $D \cong 1.5 \times 10^{-5}$ cm^2 s^{-1} in good agreement with the value of D for Pb^{2+} ions in aqueous H_2SO_4 solutions at concentrations comparable to those used in this work[6].

From the current transient at the ring and the value of N_T, the fraction of the total current at the disc related to Pb(II) soluble species was found to be less than 0.2%, coincident with the voltammetric measurements. Therefore, the correction for the contribution of Pb(II) soluble species to the current transients at the disc can be disregarded.

4. *SEM micrographs*

SEM micrographs of Pb electrode which were held at different E_f values, exhibit a large number of well defined crystals which are similar to those shown previously in the literature[5]. N_s, the density of these crystals, increases with the applied potential, in contrast to d, the average crystal size. From SEM micrographs it results that $N_s = 2.4 \times 10^{10}$ cm^{-2},

$d \cong 0.15 \pm 0.05\,\mu m$ for $E_f = -1.02\,V$ and $N_s = 6.5 \times 10^{10}\,cm^{-2}$, $d \cong 0.03 \pm 0.01\,\mu m$ for $E_f = -0.98\,V$.

DISCUSSION

These results indicate that the kinetics of the electroformation of $PbSO_4$ layers on polycrystalline Pb fits neither a solid-state nor a dissolution–precipitation simple mechanisms. It appears that the reaction involves several stages in which at least the electrodissolution of Pb to Pb^{2+} ions in solution and the $PbSO_4$ film formation through a solid-state mechanism should be included, as earlier proposed by Hall and Wright[15].

Let us consider that the average rate of the overall reaction expressed in terms of $j(t)$, the apparent instantaneous current density, can be expressed as the sum of three contributions:

$$j(t) = j_g(t) + j_d(t) + j_f(t) \quad (2)$$

where $j_g(t)$, $j_d(t)$ and $j_f(t)$ stand for the contributions of the instantaneous nucleation and growth, the Pb electrodissolution from the Pb surface fraction which is $PbSO_4$ film free, and the Pb electrodissolution through the $PbSO_4$ surface film process, respectively.

The term $j_g(t)$ can be assigned to an instantaneous nucleation and two-dimensional growth under charge-transfer control mechanism[23], *ie*

$$j_g(t) = P_1\, t \exp(-P_2\, t^2) = q_g\, d\theta'/dt \quad (3)$$

where θ' is the fractional Pb surface coverage by the $PbSO_4$ film (Fig. 9), q_g is the apparent charge density of the $PbSO_4$ layer and P_1 and P_2 are given by the following expressions:

$$P_1 = 2\pi n F M h N_0 k^2 \rho^{-1} \quad (4)$$

$$P_2 = \pi N_0 M^2 k^2 \rho^{-2} \quad (5)$$

where N_0 is the number of nuclei formed instantaneously, k is the average film growth rate constant and M, ρ and h are the molecular weight, the density and the average height of the $PbSO_4$ layer, respectively.

On the other hand, the term $j_d(t)$ should be proportional to $(1 - \theta')$, the fraction of $PbSO_4$ film free Pb surface, θ' denoting the degree of Pb surface covered by $PbSO_4$. Accordingly, $j_d(t)$ can be expressed as follows

$$j_d(t) = j_d^0(1 - \theta') \quad (6)$$

where j_d^0 stands for the Pb^{2+} electrodissolution current for $\theta' = 0$ ($t = 0$).

The term $j_f(t)$ in equation (2) emerges from the fact that at the initial stages of growth, the $PbSO_4$ thin layer behaves as an ionic conductor allowing migration of Pb^{2+} cations. These cations contribute to the growth of a $PbSO_4$ layer at the $PbSO_4$/solution interface through chemical precipitation when the concentration of Pb^{2+} cations adjacent to the electrode exceeds the supersaturation concentration. In this way passivation sets in (Fig. 9). Accordingly, as far as the Pb surface coverage by $PbSO_4$ is concerned, two different domains should be distinguished, those related to θ', the surface coverage by the $PbSO_4$ conducting layer ($0 \leqslant \theta' \leqslant 1$), and those related to θ'', the surface coverage by the $PbSO_4$ passive layer ($0 \leqslant \theta'' \leqslant \theta'$). Then, the value of $j_f(t)$ can be expressed as follows:

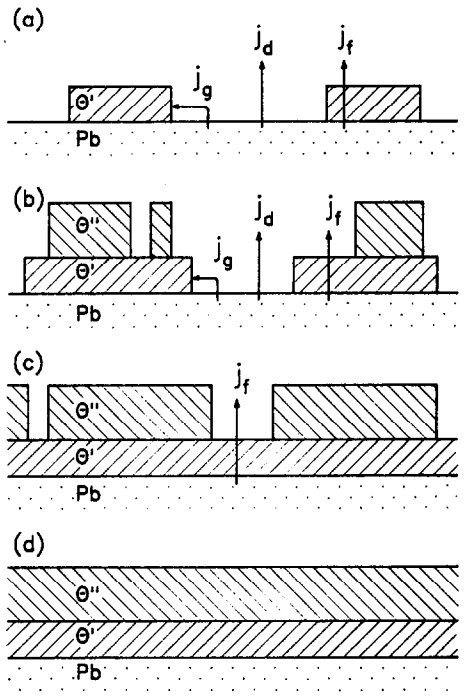

Fig. 9. Scheme of cross-sections of the electrode during the passivation process. [:.:.:] Pb; [///] $PbSO_4$ conducting layer (θ'); [\\\] $PbSO_4$ passivation layer (θ''). The different anodic current contributions are indicated. From (a) to (d) the successive stages of the anodic layer growth are indicated.

$$j_f(t) = 2F k_f(\theta' - \theta'') \quad (7)$$

where $\theta'' \leqslant \theta'$. Equation (7) indicates an increase in $j_f(t)$ with the surface coverage degree by the conducting layer and a decrease in $j_f(t)$ produced by θ'', *ie* by the surface coverage due to a true passivating layer. The rate of surface blockage due to the passive film (θ'') can be tentatively expressed by the following equation:

$$d\theta''/dt = k_p(\theta' - \theta''). \quad (8)$$

On the basis of equations (2), (3), (6), (7) and (8) using non-linear fit routines, the experimental potentiostatic transients can be reasonably reproduced with the set of parameters assembled in Table 1 (Fig. 10). The evolution of θ' and θ'' during the anodic current transient recorded at $E_f = -0.960\,V$ is illustrated in Fig. 11. The parametric relationships depend on whether the applied potential is positive or negative with respect to $-0.985\,V$, *ie* the potential at which the greatest dissolution of Pb^{2+} ions at the ring electrode is detected. At potentials lower than $-0.985\,V$, the log P_i(i = 1, 2) vs. E_f plots approach a linear relationship with a slope of $0.010 \pm 0.002\,V\,decade^{-1}$, whereas at potentials greater than $-0.985\,V$ the slopes are $0.040 \pm 0.002\,V\,decade^{-1}$ and $0.034 \pm 0.002\,V\,decade^{-1}$, respectively.

Furthermore, h, the conducting film thickness, can be estimated from equations (4) and (5) using

Table 1. Fitting parameters resulting in the E_f range covered in this work

E_f (V)	P_1 ($mA\,cm^{-2}\,s^{-1}$)	P_2 (s^{-2})	j_d^0 ($mA\,cm^{-2}$)	k_f ($10^{-8}\,mol\,cm^{-2}\,s^{-1}$)	k_p (s^{-1})
−1.020	0.00367	0.00125	0.1485	0.2138	0.00821
−1.015	0.0804	0.00720	0.2437	0.7991	0.0266
−1.010	0.0400	0.0282	0.3186	0.9774	0.0466
−1.000	0.1580	0.1580	0.9989	2.4868	0.1290
−0.990	2.0380	0.5350	1.2439	5.3716	0.3530
−0.980	7.9853	1.4339	2.1734	7.9324	0.9360
−0.970	38.380	3.2582	7.9919	4.8313	1.0257
−0.960	95.390	6.9863	15.677	6.6328	1.1840
−0.950	217.57	17.069	23.775	9.1230	2.5025
−0.940	519.64	57.544	37.527	10.049	3.1668
−0.930	837.92	91.411	54.864	5.2721	4.1164
−0.920	1200.9	156.75	88.238	6.2203	4.8438
−0.900	2004.9	355.71	124.73	8.3836	5.9801
−0.880	4375.2	1518.4	185.51	7.0034	9.0872

$M = 303\,g\,mol^{-1}$ and $\rho = 6.2\,g\,cm^{-3}$ for $PbSO_4$ (Fig. 12). In the $-1.02 \leqslant E_f \leqslant -0.99\,V$ range, the value of h becomes nearly constant, $h = 1.5 \pm 0.5\,nm$, it increases abruptly in the $-0.99 \leqslant E_f \leqslant -0.98\,V$ range, reaching a maximum value, $h = 20\,nm$, and later decreases almost linearly with E_f. This behaviour agrees with data reported earlier[11, 25]. Furthermore, these results are consistent with SEM micrographs showing that as E_f is increased, the $PbSO_4$ film becomes tight and more compact, exhibiting the formation of small and well defined $PbSO_4$ crystals.

The potential dependence of j_d^0, the current at $\theta' = 0$ ($t = 0$), fulfils a Tafel equation, with a slope, $(\partial E/\partial \log j_d^0) = 0.030 \pm 0.002\,V\,decade^{-1}$ at low potentials, and it shows the trend to approach the slope $0.120\,V\,decade^{-1}$ for $E_f > -0.94\,V$. These values of the Tafel slope agree with the initial reversible behaviour of the $Pb \leftrightarrow Pb^{2+} + 2e^-$ reaction at small anodic overpotentials[26]. It is likely that the initial reaction becomes activation controlled at high anodic overvoltages, but no firm conclusion in this respect can be provided with the present results.

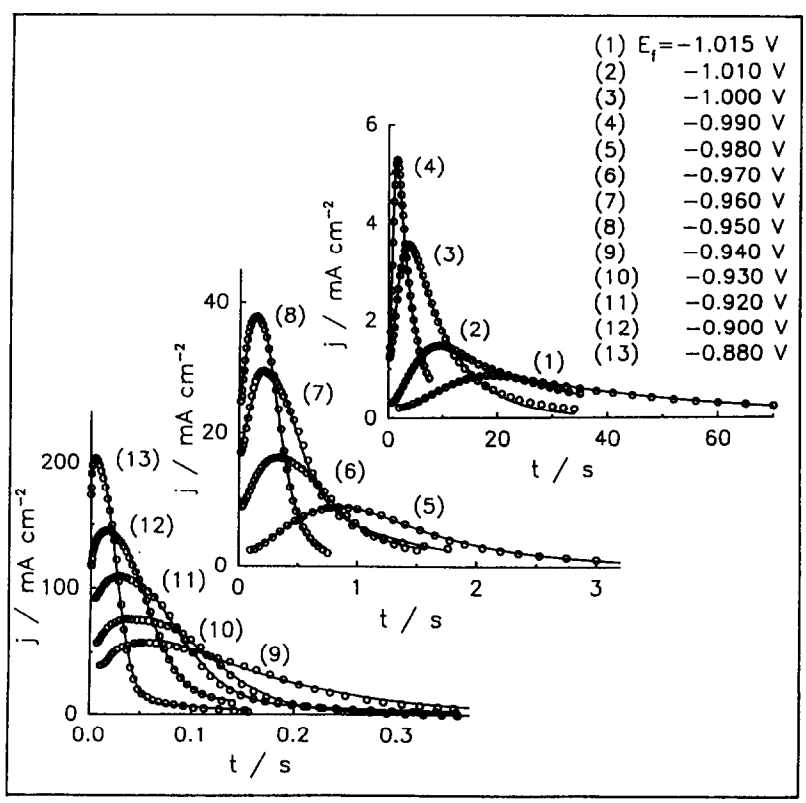

Fig. 10. Fitting of current transient data taken from Fig. 6 (full traces). Fitting parameters are given in Table 1.

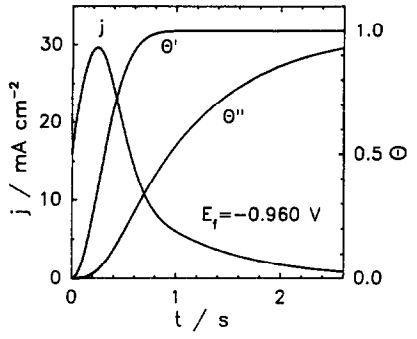

Fig. 11. Simulated evolution of θ' and θ'' during the anodic current transient recorded at $E_f = -0.960$ V.

The potential dependence of the rate constant k_f shows that for $E \geqslant -0.985$ V, the value is nearly constant, $k_f \cong (7 \pm 3) \times 10^{-8}$ mol cm^{-2} s^{-1}, whereas for $E \leqslant -0.985$ V the k_f values decrease with a slope $\Delta E/\Delta \log k_f = 0.023$ V decade^{-1}. As one would expect, the value of $(2Fk_f)$, which represents the dissolution of the electrode surface when the conducting film has grown, becomes smaller than that obtained through the fitting of j_d^0. Nevertheless, as the transfer of cations through the film is a slow process, the contribution of j_f explains the slow decay of current following the current peak.

Finally, the value of k_p related to the nonconducting $PbSO_4$ layer formation, exhibits a complex potential dependence (Table 1), which at present is difficult to interpret because of the uncontrolled precipitation of Pb^{2+} ions as $PbSO_4$ from the solution nearest to the electrode.

CONCLUSIONS

Pb passivation in sulphuric acid aqueous solutions implies processes in parallel leading to the formation of a two layer $PbSO_4$ structure. The inner conducting layer consists of a disordered crystalline phase, which is formed following an instantaneous nucleation and two-dimensional growth under charge-transfer control. Pb dissolution can continue by the diffusion of cations through this conducting layer and, when the concentration in solution is greater than the critical supersaturation limit, it tends to reprecipitate back onto the surface to form a highly crystalline $PbSO_4$ layer which passivates the electrode.

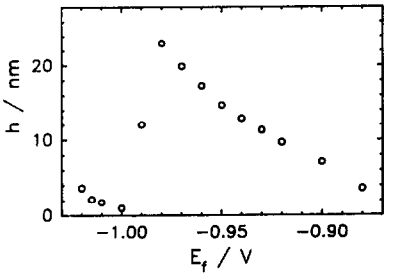

Fig. 12. Dependence of h on E_f. Data related to parameters P_1 and P_2 assembled in Table 1.

Acknowledgements—This research project was financially supported by the Consejo Nacional de Investigaciones Científicas y Técnicas, the Comisión de Investigaciones Científicas de la Provincia de Buenos Aires and the Fundación Antorchas.

REFERENCES

1. J. Burbank, A. C., Simon and E. Willihnganz, in *Advances in Electrochemistry and Electrochemical Engineering* (Edited by P. Delahay and C. Tobias), Vol. 8, pp. 157–251. John Wiley, New York (1971).
2. T. F. Sharpe, in *Encyclopedia of Electrochemistry of the Elements* (Edited by A. J. Bard), Vol. 1, pp. 235–347. Marcel Dekker, New York (1973).
3. H. Bode, *Lead–Acid Batteries*, John Wiley, New York (1977).
4. D. Berndt, in *Comprehensive Treatise of Electrochemistry* (Edited by J. O'M. Bockris, B. E. Conway, E. Yeager and R. E. White), Vol. 3, pp. 371–384. Plenum Press, New York (1981).
5. K. R. Bullock and D. Pavlov (Editors), *Advances in Lead–Acid Batteries*, The Electrochemical Society Inc., Pennington, New Jersey (1984).
6. G. Archdale and J. A. Harrison, *J. electroanal. Chem.* **34**, 21 (1972); **39**, 357 (1972).
7. A. N. Fleming and J. A. Harrison, *Electrochim. Acta* **21**, 905 (1976).
8. D. Pavlov, *Electrochim. Acta* **13**, 2051 (1968); **23**, 845 (1978).
9. D. Pavlov and R. Popova, *Electrochim. Acta* **15**, 1483 (1970).
10. D. Pavlov and N. Iordanov, *Electrochim. Acta* **117**, 1103 (1970).
11. N. A. Hampson and J. B. Lakeman, *J. electroanal. Chem.* **107**, 177 (1980).
12. V. Danel and V. Plichon, *Electrochim. Acta* **28**, 785 (1983).
13. S. Fletcher and D. B. Matthews, *J. appl. Electrochem.* **11**, 1 (1981); **11**, 23 (1981).
14. L. M. Baugh, K. L. Bladen and F. L. Tye, *J. electroanal. Chem.* **145**, 355 (1983).
15. S. B. Hall and G. A. Wright, *Corros. Sci.* **31**, 709 (1980).
16. C. V. D'Alkaine and J. M. Cordeiro, in *Advances in Lead–Acid Batteries*, p. 190. The Electrochemical Society Inc., Pennington, New Jersey (1984).
17. F. E. Varela, O. A. Albani, L. M. Gassa and J. R. Vilche, *Proc. VII Symp. Bras. Electrochem. Electroanal.* pp. 482–497. University of Sao Paulo, Sao Paulo (1990).
18. M. E. Vela, F. E. Varela, J. R. Vilche and A. J. Arvia, *Ext. Ab. IX Iberoam. Congr. Electrochem.* pp. 494–499. University of La Laguna, Tenerife (1990).
19. F. E. Varela, L. M. Gassa and J. R. Vilche, *Electrochim. Acta* **37**, 1119 (1992).
20. Iv. V. Pleskov and V. Iv. Filinovskii, *The Rotating Disc Electrode*, Consultants Bureau, New York (1976).
21. Z. Galus, in *Standard Potentials in Aqueous Solution* (Edited by A. J. Bard, R. Parsons and J. Jordan), pp. 220–235. Marcel Dekker, New York (1985).
22. A. J. Calandra, N. R. de Tacconi, R. Pereiro and A. J. Arvia, *Electrochim. Acta* **19**, 901 (1974).
23. J. A. Harrison and H. R. Thirsk, in *Advances in Electroanalytical Chemistry* (Edited by A. J. Bard), Vol. 5, pp. 67–148. Marcel Dekker, New York (1971).
24. S. Bruckenstein and G. A. Feldman, *J. electroanal. Chem.* **9**, 395 (1965).
25. M. Fleischmann and H. R. Thirsk, *Trans. Faraday Soc.* **51**, 71 (1955).
26. N. A. Hampson, C. Lazarides, G. M. Bulman and C. Knowles, in *Power Sources* (Edited by J. Thompson), Vol. 8, pp. 621–630. Academic Press, London (1981).